

Nonmagnetic impurities and roughness effects on the finite temperature magnetic properties of core-shell spherical nanoparticles

E. Vatansever* and Y. Yüksel

Department of Physics, Dokuz Eylül University, Tinaztepe Campus, TR-35160 Izmir, Turkey

(Dated: October 5, 2018)

Being inspired by a recent study [V. Dimitriadis et al. Phys. Rev. B **92**, 064420 (2015)], we study the finite temperature magnetic properties of the spherical nanoparticles with core-shell structure including quenched (i) surface and (ii) interface nonmagnetic impurities (static holes) as well as (iii) roughened interface effects. The particle core is composed of ferromagnetic spins, and it is surrounded by a ferromagnetic shell. By means of Monte Carlo simulation based on an improved Metropolis algorithm, we implement the nanoparticles using classical Heisenberg Hamiltonians. Particular attention has also been devoted to elucidate the effects of the particle size on the thermal and magnetic phase transition features of these systems. For nanoparticles with imperfect surface layers, it is found that bigger particles exhibit lower compensation point which decreases gradually with increasing amount of vacancies, and vanishes at a critical value. In view of nanoparticles with diluted interface, our Monte Carlo simulation results suggest that there exists a region in the disorder spectrum where compensation temperature linearly decreases with decreasing dilution parameter. For nanoparticles with roughened interface, it is observed that the degree of roughness does not play any significant role on the variation of both the compensation point and critical temperature. However, the low temperature saturation magnetizations of the core and shell interface regions sensitively depend on the roughness parameter.

PACS numbers: 75.75.-c, 75.30. Kz, 61.43. Bn, 68.35. Ct

Keywords: Core-shell nanoparticles, roughness effects, nonmagnetic impurities, Monte Carlo simulation.

I. INTRODUCTION

When the size of a magnetic system is reduced to a characteristic length, the system has a bigger surface to volume ratio giving rise to a great many outstanding thermal and magnetic properties compared to the conventional bulk systems [1]. Advanced functional magnetic nanostructures in different geometries, such as nanowires, nanotubes, nanospheres, nanocubes are center of interest because of their technological [2, 3] and scientific importance as well as biomedical applications [4–6]. From the experimental point of view, many studies have been carried out to discuss and understand the origin of the fascinating physical properties observed in magnetic nanoparticles [6–10]. For example, recently the multi-functional core-shell nanowires have been synthesized by a facile low-cost fabrication process [6]. Based on this study, it has been shown that a multidomain state at remanence can be obtained, which is an attractive feature for the biomedical applications. In another interesting study, the authors show the presence of a robust antiferromagnetic coupling between core and shell in ferrimagnetic soft/hard and hard/soft core-shell nanoparticles based on Fe-oxides and Mn-oxides [9]. They have also used a computational model to support the physical facts observed in the experiment. Moreover, it is a fact that core-shell nanoparticle systems exhibit two important phenomena, namely exchange bias and magnetic proximity effects. These are completely due to the interface effects of the system. For detailed reviews on the exchange bias and magnetic proximity phenomena, the readers may follow the references [11–15].

Ferrimagnetic materials have a compensation temperature under certain conditions. At this special temperature region, the net magnetization of the sample vanishes below its critical temperature [16]. The phenomenon of ferrimagnetism in bulk material is associated with the counteraction of opposite magnetic moments with unequal magnitudes located on different sublattices in the same system. According to the Refs. [17, 18], interestingly coercive field presents a behavior with a rapid increment at the compensation point. Existence of such a point has a technological importance [19, 20], because at this point only a small magnetic field is required and enough to change the sign of the net magnetization. However, the origin of the compensation point found in the nanostructures is quite different from those observed in the ferrimagnetic bulk materials. Magnetic nanoparticles can exhibit a compensation point due to the existence of an antiferromagnetic interface coupling at the ferromagnetic core and ferromagnetic shell interface even if the lattice sites in the core and shell parts of the system are occupied by identical atomic spin moments. Hence,

*Electronic address: erol.vatansever@deu.edu.tr

investigation of ferrimagnetism in nanoparticle systems has opened a new and an intensive field in the research of the critical phenomena in magnetic nanoparticles. For example, the critical and compensation temperatures properties of cylindrical nanowire and nanotube systems have been performed by means of Effective-Field Theory with single-site correlations [21, 22]. In these studies, the authors have also focused their attention on the effects of the surface and its dilution on the magnetic properties of the considered system, and it is reported that these systems display a compensation point for appropriate values of the system parameters. Very recently, thermal and magnetic phase transition features of a core-shell spherical nanoparticle with binary alloy shell have been studied by making use of Monte Carlo simulation based on single-spin flip Metropolis algorithm [23]. Here, the authors claim that the system may demonstrate one, two or even three compensation points depending on the selected Hamiltonian as well as on the concentration parameters. In addition to these, critical behaviors of core-shell nanoparticles with ferromagnetic materials but with antiferromagnetic interface exchange coupling are studied by means of a self-consistent local mean-field analysis [24]. It has been found that compensation temperature depends on all the material parameters, namely the core and shell radius, and the magnetic field.

Although the mechanism and physics underlying of the critical behavior of the magnetic nanoparticles may be treated and understood with idealized interfaces and surfaces of the nanoparticle, real magnetic nanoparticles have some small defects. From this point of view, experimental systems showing exchange bias may contain statistical distributions due to the presence of randomly located defects in the system [25, 26]. Recently, Ho and co-workers have attempted to address the magnetic properties of a ferromagnetic/antiferromagnetic core-shell nanospherical particle including the vacancies at the antiferromagnetic interface, based on Monte-Carlo simulation method [27]. It is found that the frustrated spins at the ferromagnetic interface is another pinning-source generating exchange bias phenomenon, in addition to the antiferromagnetic shell spins. Furthermore, the influences of non-magnetic defects on the exchange bias of core-shell nanoparticles have been analyzed by benefiting from Monte Carlo simulation, and it is shown that exchange bias can be tuned by defects in different positions [28]. Apart from these, Evans et al. [25] presented exchange-bias calculations for FM core/AFM shell nanoparticles with roughened interfaces. They showed that the magnitude of exchange bias is strongly correlated with the degree of roughness. Moreover, in a very recent paper, Dimitriadis et al. [29] simulated cubic and spherical particles showing exchange bias phenomenon. According to their results, in terms of exchange bias characters, the distinction between cubic and spherical particles is lost for moderate roughness.

Based on the previously published studies, it is possible to mention that thermal and magnetic properties of the core-shell nanoparticles containing the surface and interface defects and also roughened interfaces are complicated and interesting compared to the clean nanoparticle systems. It is certain that the studies taking these effects into account play a crucial role in having a better insight of the physics behind real magnetic nanoparticle systems. However, much less attention has been given to determine the influences of the disorder and roughness on the critical behavior of the core-shell nanoparticles, and there are still many unresolved issues. Motivated by these facts, we intend to search answers for the following questions:

- What are the effects of the nonmagnetic impurities at the surface and interface of a core-shell type spherical nanoparticle on the critical and compensation behavior ? Is it possible to control the magnetic behavior of the core-shell nanoparticles by means of concentration of the vacancies ?
- What kind of physical relationships may emerge between the physical properties of the system and the interface roughness ?

The main motivation of the paper is to make an attempt to determine the physical facts underlying these questions. Furthermore, particular attention has been dedicated to elucidate the effects of the system size on the critical behavior of the system. We believe that the findings obtained in this work would be beneficial for the future theoretical and experimental research in magnetic nanoparticles including disorder effects.

The outline of the remainder parts of the paper is as follows: In section II, we present the model and simulation details. The results and discussion are given in section III, and finally section IV includes our conclusions.

II. MODEL AND SIMULATION DETAILS

We consider a spherical nanoparticle which has been schematically depicted in Fig. 1 with a FM core which is surrounded by a FM shell. At the core-shell interface (which is composed of the outermost core and the innermost shell layers) we define an AFM exchange coupling. The interface region consists of two successive monolayers. The total radius of the particle and the thickness of the shell are denoted by R and R_S , respectively. A classical Heisenberg spin resides at each lattice site of a simple cubic structure, and the nearest neighbor sites are separated from each

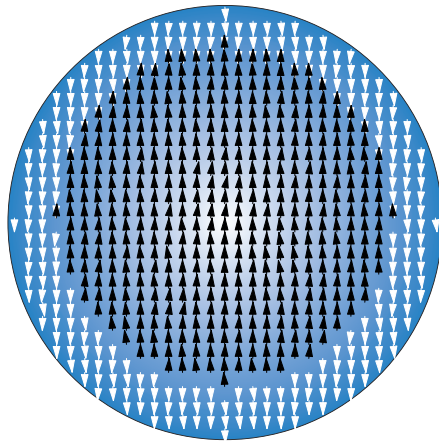


FIG. 1: Schematic representation of an ideally purified spherical nanoparticle composed of classical Heisenberg spins. FM core of radius R_c is coated by an FM shell of thickness R_S . Total radius of the particle is denoted by $R = R_c + R_S$. At the interface, the outermost core and the innermost shell layers interact with an AFM exchange coupling.

other by unitary lattice spacing. The system can be defined according to the following Hamiltonian

$$\mathcal{H} = -J_C \sum_{\langle ij \rangle} \mathbf{S}_i \cdot \mathbf{S}_j - J_S \sum_{\langle kl \rangle} \mathbf{S}_k \cdot \mathbf{S}_l - J_{IF} \sum_{\langle jk \rangle} \mathbf{S}_j \cdot \mathbf{S}_k - K_C \sum_i (S_i^z)^2 - K_S \sum_k (S_k^z)^2, \quad (1)$$

where \mathbf{S}_i represents a classical Heisenberg spin vector with unit magnitude, and the former three sums are taken over the nearest-neighbor sites whereas remaining terms are taken over all the lattice sites. In practice, spin structure of interface in such systems is experimentally inaccessible, and it is quite a challenge to determine the magnetic nature near interface. Therefore, in order to theoretically investigate the ferrimagnetic properties of the system, we consider the following Hamiltonian parameters: Spin-spin interactions between core and shell spins are taken as ferromagnetic ($J_{C,S} > 0$) whereas interactions at the core-shell interface are of antiferromagnetic type ($J_{IF} < 0$). Due to the reduced coordination number at the surface, FM exchange interactions between shell spins are usually smaller than those between core spins. Hence, we select $J_S = 0.5J_C$ with $|J_{IF}| \leq 2.0J_C$. Easy axis magnetization of the particle is assumed to be along the z direction by assigning nonzero values for the z components of the uniaxial anisotropy constants K_C and K_S for the particle core and shell, respectively. In order to emphasize the surface effects, we set $K_C = 0.1J_C = 0.1K_S$ [30].

A variety of values for the total radius has been considered as $R = 10.0, 15.0, 20.0, 25.0$ and 30.0 throughout the simulations, corresponding to the particles with $N_T = 4169, 14147, 33401, 65267$ and 113081 spins, respectively. However, in most cases, the shell thickness has been varied at the expense of the core which mimics the case of the production process for the surface chemically modified nanoparticles [13]. Our simulations are based on an improved Metropolis algorithm for classical Heisenberg spins [31–33], and we apply free boundary conditions in all directions.

Following physical quantities have been calculated in the simulation process:

- Thermal and configurational averages of the instantaneous magnetizations,

$$\begin{aligned} M_C^\alpha &= \frac{1}{N_C} \left\langle \sum_{i=1}^{N_C} S_i^\alpha \right\rangle, \\ M_S^\alpha &= \frac{1}{N_S} \left\langle \sum_{i=1}^{N_S} S_i^\alpha \right\rangle, \\ M_{IF}^\alpha &= \frac{1}{N_{IF}} \left\langle \sum_{i=1}^{N_{IF}} S_i^\alpha \right\rangle, \\ M_T^\alpha &= \frac{1}{N_T} \left\langle \sum_{i=1}^{N_T} S_i^\alpha \right\rangle \quad \text{with } \alpha = x, y, z. \end{aligned} \quad (2)$$

where M_C^α , M_S^α , M_{IF}^α , M_T^α denote the average magnetizations corresponding to core, shell, interface parts, and total system, respectively with corresponding number of lattice sites N_C , N_S , N_{IF} and N_T which depend on the

shell thickness and the total radius of the particle. Hence, using Eq. (2), the magnitude of the magnetization vector can be computed via

$$M_\delta = \sqrt{(M_\delta^x)^2 + (M_\delta^y)^2 + (M_\delta^z)^2}, \quad \delta = C, S, IF \text{ or } T \quad (3)$$

for any distinct region of the particle.

- Internal energy and specific heat per lattice site can also be calculated using

$$E_{\text{total}} = -\langle \mathcal{H} \rangle / N_T, \quad C = \frac{dE_{\text{total}}}{dT}. \quad (4)$$

In order to calculate the temperature dependence of magnetization and specific heat curves, we have performed simulations with 5×10^4 steps at each temperature. In order to allow the system to reach a stationary state, we have discarded the first 25% steps for thermalization. In the calculations, we set $k_B = 1$ for simplicity.

III. RESULTS AND DISCUSSION

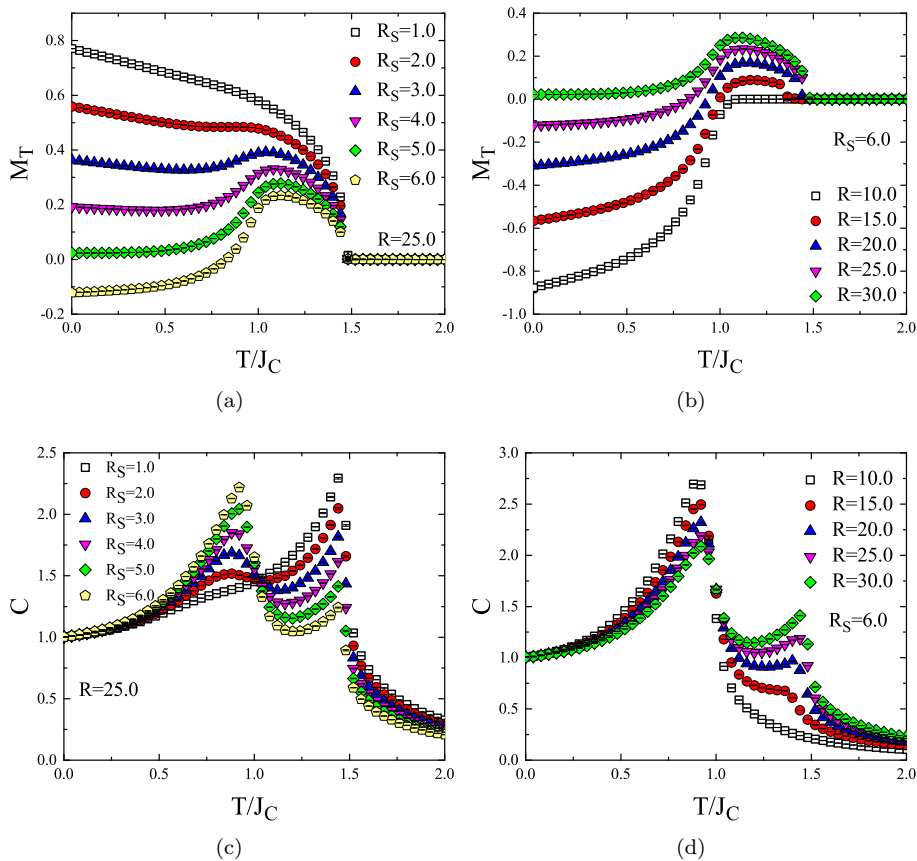


FIG. 2: Temperature variation of total magnetization M_T and specific heat C corresponding to simulated pure nanoparticle samples with some selected values of shell thickness R_S and total radius R . The results have been obtained for the following system parameters: $J_S = 0.5J_C$, $J_{IF} = -0.5J_C$, $K_C = 0.1J_C$, $K_S = 1.0J_C$.

In this section, let us discuss the results for the particles with disordered surface and interfaces. However, before presenting these results, it would be beneficial to take a glance at the magnetic properties of the pure system. The results for the total magnetization M_T and specific heat per spin C as a function of temperature, as well as the shell and overall particle sizes are shown in Fig. 2. These results have been obtained after averaging over 10 different sample realizations at each temperature. The error bars obtained via Jackknife method [34] are smaller than the data symbols. As shown in this figure, nanoparticles with different structural parameters may exhibit different magnetization profiles.

Namely, according to the Néel classification scheme, thermal dependence of magnetization curves can be classified in several categories. For instance, as shown in Fig. 2a, the magnetization curves exhibit Q, P, L, N type behaviors with increasing shell thickness in successive order whereas for fixed shell thickness, such as $R_S = 6.0$, we obtain Q, N, L, P type of behaviors, respectively for increasing total radius R , (c.f. see Fig 2c). The existence of N type magnetization profiles is important in technological applications [35].

From Figs. 2c and 2d, it can be deduced that the specific heat curves may exhibit two successive maximum points. Those observed at low temperature region originates due to the thermal fluctuations in the shell, however the high temperature peak is a consequence of the thermal variation of the core magnetization. The magnitude of the both peaks are size dependent: core (shell) peak with a cusp-like divergent behavior becomes a broadened hump as the core (shell) magnetization loses its dominance with varying system size. We also note that the temperature value corresponding to the peak located at high temperature region is the sole transition temperature [36] since, the system becomes completely paramagnetic above this temperature.

After presenting this general overview of the pure case, let us discuss the effects of disorder due to the surface and interfacial impurities, as well as roughened interfaces. Due to its technological importance, we will focus our attention on the variation of compensation behavior [37] of the system in the presence of above mentioned disorder effects.

A. Nanoparticles with Imperfect Shell Layers

Nanoparticle system in the presence of surface disorder can be simulated by considering randomly distributed non-magnetic sites on the surface and in the interior regions of the shell layer (except the innermost shell sites which are located at the core-shell interface region). In this case, the modified Hamiltonian defining the system reads

$$\mathcal{H} = -J_C \sum_{\langle ij \rangle} \mathbf{S}_i \cdot \mathbf{S}_j - J_S \sum_{\langle kl \rangle} \mathbf{S}_k \cdot \mathbf{S}_l \zeta_k \zeta_l - J_{IF} \sum_{\langle jk \rangle} \mathbf{S}_j \cdot \mathbf{S}_k - K_C \sum_i (S_i^z)^2 - K_S \sum_k \zeta_k (S_k^z)^2, \quad (5)$$

where ζ_k is the site occupancy parameter which takes values zero or unity, depending on whether the lattice site k exhibits nonmagnetic or magnetic character, respectively. In this manner, the total amount of disorder is controlled with a parameter p , such that $p = 1.0$ means all the lattice sites in the particle shell are magnetic whereas $p = 0.0$ means that no magnetic lattice points reside in the outer shell, and in this case, the only contribution for the shell magnetization comes from the innermost shell spins (i.e. from the interfacial shell spins).

Taking the above mentioned model as a basis, we plot the phase diagrams in a $(T_C/J_C, T_{comp}/J_C)$ versus p plane in Fig. 3 for three different total radius values such as $R = 15.0, 20.0$ and 25.0 with a fixed shell thickness $R_S = 6.0$. The horizontal data in Fig. 3 denotes the transition temperature of the system which is not affected from the dilution of the shell region by non magnetic impurities. As shown in Fig. 2b, this system exhibits a compensation point below the transition temperature in the absence of disorder. By examining Fig. 3, one can see that bigger particles exhibit lower compensation point T_{comp} which decreases gradually with increasing disorder, and vanishes at a critical p_c value. Besides, the compensation frontier in the phase diagram reaches to stronger disorder regime for smaller particles.

The representative plots for color-maps of total magnetization $|M_T|$ and the specific heat C with $R = 25.0$ and $R_S = 6.0$ corresponding to the phase diagrams depicted in Fig. 3 are given in Fig. 4. According to Fig. 4a, the compensation behavior originates in the low temperature and weak disorder region, since the particle size is relatively big. At very low temperatures, the total magnetization can be calculated from $|M_T| = |(N_C M_C + N_S M_S)|/N_T$, hence it reaches its maximal value when the shell magnetization is weak due to AFM exchange at the interface. In this context, by taking the AFM structure of the interface exchange coupling into account, we have $N_C = 28671$, $N_S = 36596$ for a perfectly pure particle ($p = 1.0$). Therefore, it yields $|M_T| = 0.121$, whereas for fully imperfect case ($p = 0.0$), for $N_C = 28671$ and $N_S = N_S^{IF} = 3854$, we find $|M_T| = 0.38$ which agrees well with the results shown in Fig. 4a. According to the Néel classification scheme [16], M_T exhibits N, L, P , and Q type of behaviors with increasing disorder. From Fig. 4b, it is clear that the specific heat exhibits two successive peaks for $p = 1.0$. However, as the amount of magnetic lattice sites in the shell progressively decreases then the lower temperature peak tends to disappear. Apart from these, both from Fig. 4a and 4b, one should notice that the transition temperature of the system is located around $T_C \approx 1.5J_C$, and it is insensitive to the presence of shell disorder, since the major contribution to the magnetism of the particle mainly comes from the core part.

B. Nanoparticles with Diluted Interface

In this subsection, we discuss and present results for nanoparticles with disordered interface sites. In this regard, one should modify the Hamiltonian given in Eq. (1) as

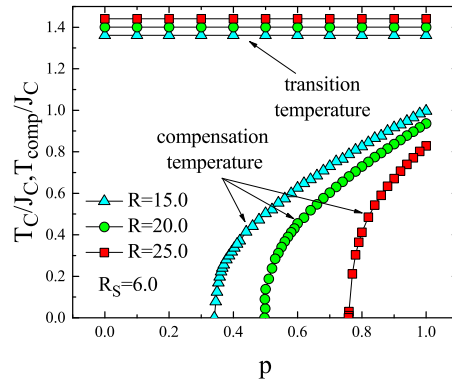


FIG. 3: The phase diagrams in a $(p - T_C/J_C, T_{comp}/J_C)$ plane for the simulated particles with $R_S = 6.0$, $R = 15.0, 20.0, 25.0$. The other system parameters are fixed as: $J_S = 0.5J_C$, $J_{IF} = -0.5J_C$, $K_C = 0.1J_C$, $K_S = 1.0J_C$.

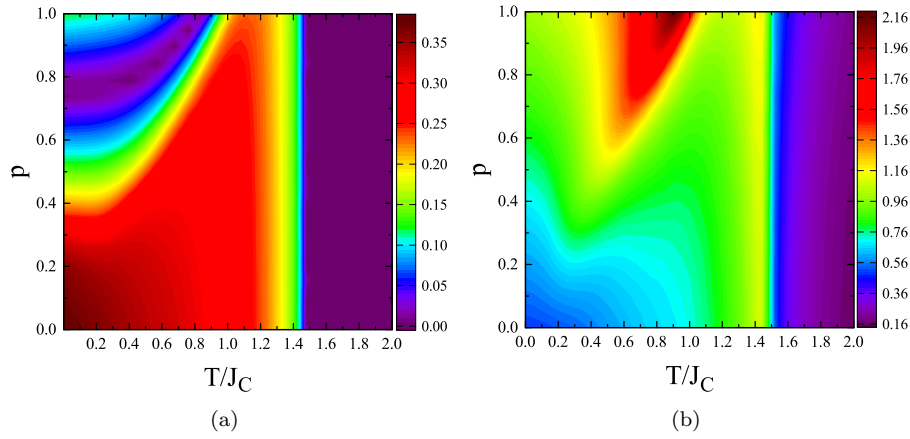


FIG. 4: The color map contour plots of (a) the total magnetization $|M_T|$, (b) specific heat C for the system with $R = 25.0$ and $R_S = 6.0$ corresponding to the phase diagram depicted in Fig. 3. The other fixed system parameters are as follows: $J_S = 0.5J_C$, $J_{IF} = -0.5J_C$, $K_C = 0.1J_C$, $K_S = 1.0J_C$.

$$\mathcal{H} = -J_C \sum_{\langle ij \rangle} \mathbf{S}_i \cdot \mathbf{S}_j \zeta_j - J_S \sum_{\langle kl \rangle} \mathbf{S}_k \cdot \mathbf{S}_l \zeta_k - J_{IF} \sum_{\langle jk \rangle} \mathbf{S}_j \cdot \mathbf{S}_k \zeta_j \zeta_k - K_C \sum_i \zeta_i (S_i^z)^2 - K_S \sum_k \zeta_k (S_k^z)^2, \quad (6)$$

where ζ_k is the site occupancy parameter, as usual. p is the ratio of magnetic sites located at the core-shell interface with $p = 1.0$ and 0.0 , respectively corresponding to the cases with pure and maximally disordered situations. Fig. 5 shows the variation of compensation point T_{comp} and transition temperature T_C as functions of p for three different values of the total radius R of the particle. This figure shows that T_{comp} always decreases, but the transition temperature does not change with increasing interface disorder. There exists a region in the disorder spectrum such as $1.0 \geq p \geq p^*$ where T_{comp} linearly decreases with decreasing p such as $T_{comp} \propto \alpha p$, and the dashed lines accompanying the simulation data denote the linear fitting curves. The linear variation region becomes narrower for bigger particles. From our data we find $\alpha = 0.113, 0.065$, and 0.033 for respective radius values $R = 10.0, 15.0$, and 25.0 . The statistical error due to fitting procedure is in the order of 10^{-15} in all cases.

The representative contour plots regarding the magnetization $|M_T|$ and specific heat C as functions of temperature and parameter p are shown in Fig. 6 for $R = 25.0$ and $R_S = 6.0$ corresponding to the phase diagrams displayed in Fig. 5c. The variation of T_{comp} as a function of p around $T = 0.8J_C$ is not clearly visible since the constant of proportionality α is very small. However, the system always maintains its N type magnetization with varying p . At the ground state, when $p = 1.0$, the total magnetization $|M_T|$ is given by $|M_T| = |N_C M_C + N_S M_S|/N_T = 0.121$ as before, (see Fig. 4). On the other hand, in the maximally disordered case, among the number of $N_{IF} = 7448$ sites of the interface region, a number of $N_C^{IF} = 3594$ and $N_S^{IF} = 3854$ sites belonging to core and shell interface regions are nonmagnetic. Hence the total magnetization reads $|M_T| = |[(28671 - 3594) - (36596 - 3854)] / 65267| = 0.117$ which

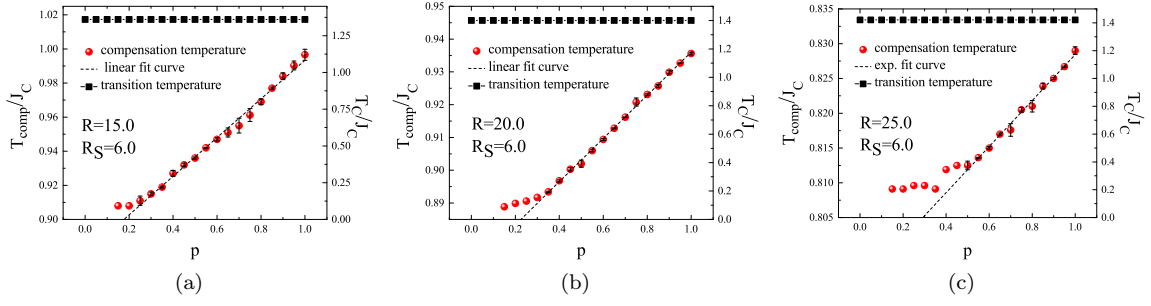


FIG. 5: Phase diagrams in a $(p - T_{comp}/J_C, T_C/J_C)$ plane for simulated particles with shell thickness $R_S = 6.0$ with three different values of the total radius (a) $R = 15$, (b) $R = 20$, (c) $R = 25$. The other system parameters are fixed as $J_S = 0.5J_C$, $J_{IF} = -0.5J_C$, $K_C = 0.1J_C$, $K_S = 1.0J_C$. The horizontal data symbols denote the transition temperature.

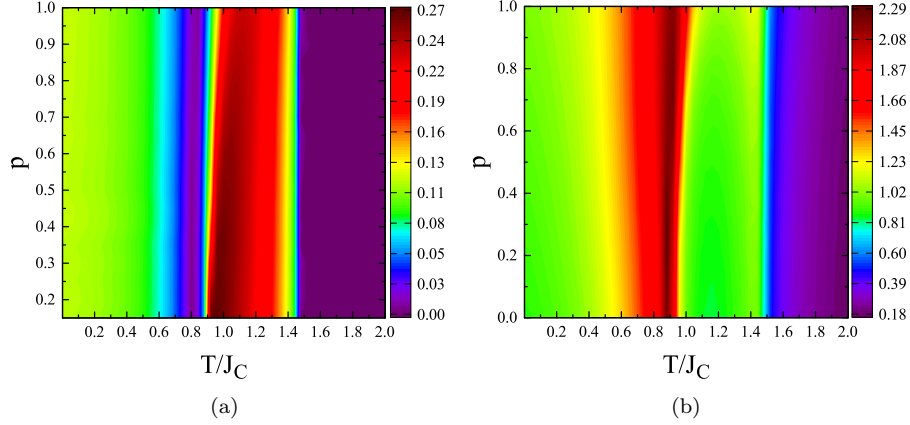


FIG. 6: The color map contour plots of (a) the total magnetization $|M_T|$, (b) specific heat C for the system with $R = 25.0$ and $R_S = 6.0$ corresponding to the phase diagram depicted in Fig. 5c. The other fixed system parameters are as follows: $J_S = 0.5J_C$, $J_{IF} = -0.5J_C$, $K_C = 0.1J_C$, $K_S = 1.0J_C$.

is in accordance with the results given in Fig. 6a. Apart from these, specific heat curves exhibit two successive peaks due to the reasons described in our previous discussions.

C. Nanoparticles with Roughened Interface

As a final investigation in this work, we consider magnetic nanoparticles with roughened interfaces in the following discussions. In order to simulate particles with rough interfaces we use a method very similar to those utilized in previous works [25, 29]. Namely, for a given shell thickness and particle radius, we determine the radius R_C of the ferromagnetic core. Then we generate a local radius R_C^i value for each interface lattice site i . This local radius is drawn from a Gaussian distribution which has variance σ , and it is centered at R_C . In this way, we sample number of N_{IF} different random variables. If the local radius R_C^i of a particular interface lattice site i satisfies the inequality $R_C + \delta \leq R_C^i \leq R_C - \delta$ then this lattice site remains unaltered. In other words, if it belongs to the core interface, it remains in there throughout the generation process for the particle shape (in our simulations, the parameter δ corresponds to 10% of the unitary lattice spacing). On the other hand, if R_C^i does not satisfy the above inequality, then we generate a random number r within the interval $[0, 1)$. If $r > 0.5$ then the i^{th} lattice site belongs to the core interface, else it is assigned to the shell interface. Using this process, amount of roughness is controlled by varying the Gaussian distribution width σ , and we successfully create roughened interfaces without producing isolated nonmagnetic sites [29].

Before proceeding further, it would be useful to clarify the effect of interface exchange coupling J_{IF} on the thermal and magnetic properties of the particle system. For this aim we prepare sample realizations corresponding to four different samples (see Table I). In Fig. 7, we show the influence of exchange coupling J_{IF} on the thermal variation of total magnetization $|M_T|$ and specific heat C curves. At first sight, it is clear that neither small nor large particles

TABLE I: Structural parameters of simulated nanoparticles with ideal interface structure.

Sample	R	R_S	N_C	N_S	N_{int}	N_C^{int}	N_S^{int}	N_T
1	25.0	2.0	50883	14384	5354	5670	11024	65267
2	25.0	6.0	28671	36596	3594	3854	7448	65267
3	15.0	2.0	9171	4976	1674	1854	3528	14147
4	15.0	6.0	3071	11076	794	918	1712	14147

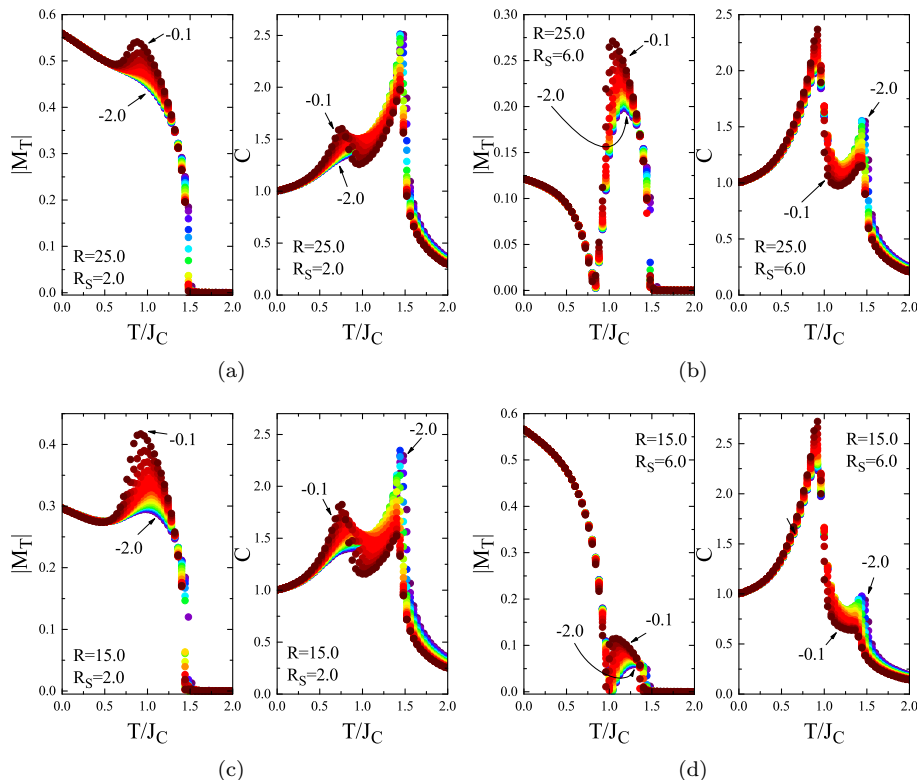


FIG. 7: Temperature dependence of the total magnetization $|M_T|$ and specific heat C for a wide variety of interfacial exchange coupling $-0.1 \geq J_{IF} \geq -2.0$. Four different samples have been prepared for simulation: (a) Sample 1 with $R = 25.0$, $R_S = 2.0$, (b) Sample 2 with $R = 25.0$, $R_S = 6.0$, (c) Sample 3 with $R = 15.0$, $R_S = 2.0$, and (d) Sample 4 with $R = 15.0$, $R_S = 6.0$. The other system parameters are fixed as $J_S = 0.5J_C$, $K_C = 0.1J_C$, $K_S = 1.0J_C$.

can exhibit a compensation point unless the shell thickness is greater than a critical value (see Fig. 2a). Furthermore, even if the system exhibits a compensation point T_{comp} , varying J_{IF} values do not alter the location of T_{comp} . A similar scenario is also valid for the transition temperature. However, varying J_{IF} values only affect the magnitude of the low temperature specific heat peaks. These aforementioned results may indicate that the interfacial roughness may have no any significant effect on the compensation phenomenon. Keeping this in mind, we prepare samples according to Table I with roughened interfaces. These structures are also schematically illustrated in Fig. 8. In Fig. 9, we depict the results for $|M_T|$ and C curves with four distinct samples corresponding to Fig. 8 from which one can deduce that the degree of roughness does not play any significant role on the variation of both the compensation point and critical temperature. This result supports our predictions based on Fig. 7. Finally, let us show how the interface magnetizations regarding the core and shell regions are affected from the roughness effects. In this context, Fig. 10 concludes that increasing amount of roughness does not alter the transition temperature of the system, but reduces the low temperature saturation magnetizations of the core and shell interface regions.

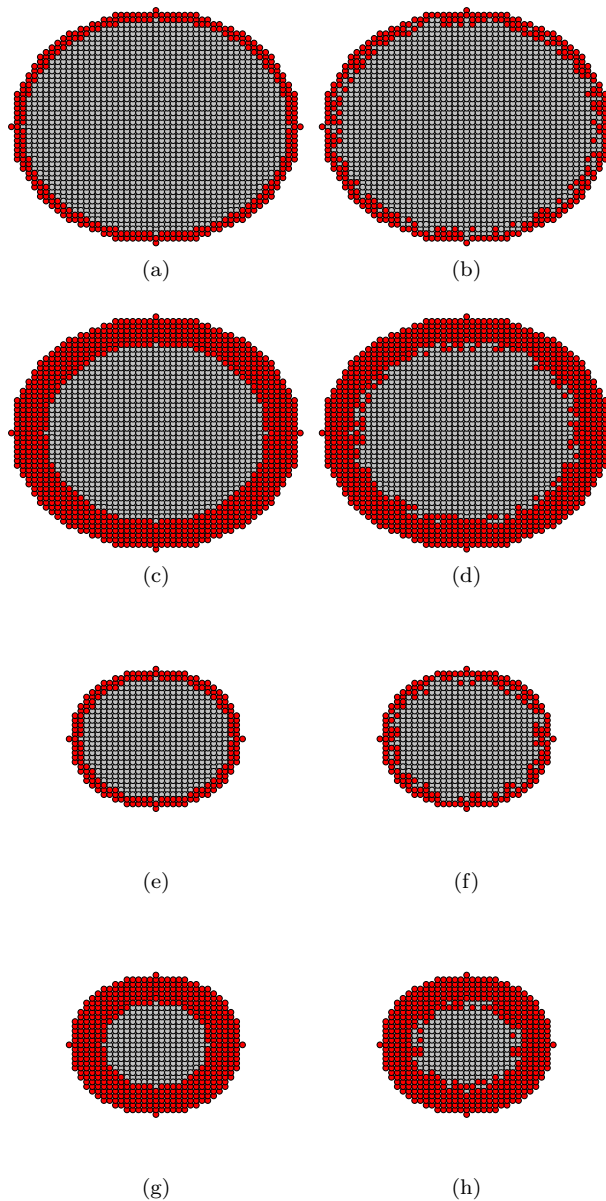


FIG. 8: Schematic representation of 2D cross-sections of the simulated particles with structural parameters enlisted in Table I. The left and right columns show four different samples with or without roughness, respectively. (a), (b): Sample 1; (c), (d): Sample 2; (e), (f): Sample 3; (g), (h): Sample 4. $\sigma = 1.0$ is used for generating the roughened particle interfaces.

IV. CONCLUDING REMARKS

In conclusion, by benefiting from Monte Carlo simulation based on an improved Metropolis algorithm, we carry out a systematic investigation to elucidate the finite temperature magnetic properties of core-shell spherical nanoparticles containing quenched surface and interface disorders as well as roughened interface effects. Some efforts have also been taken to study the particle size effects on the thermal and magnetic properties of the particles. After a detailed numerical analysis, most prominent observations underlined in the present work can be briefly summarized as follows:

- For core-shell spherical nanoparticles with imperfect surface layers, it is found that bigger particles exhibit lower compensation point which decreases gradually with increasing amount of vacancies, and vanishes at a critical value. In view of the specific heat treatment as a function of the temperature, the specific heat demonstrates two successive peaks for clean case, namely $p = 1.0$. However, as the amount of magnetic lattice sites in the shell progressively decreases then the lower temperature peak tends to disappear.

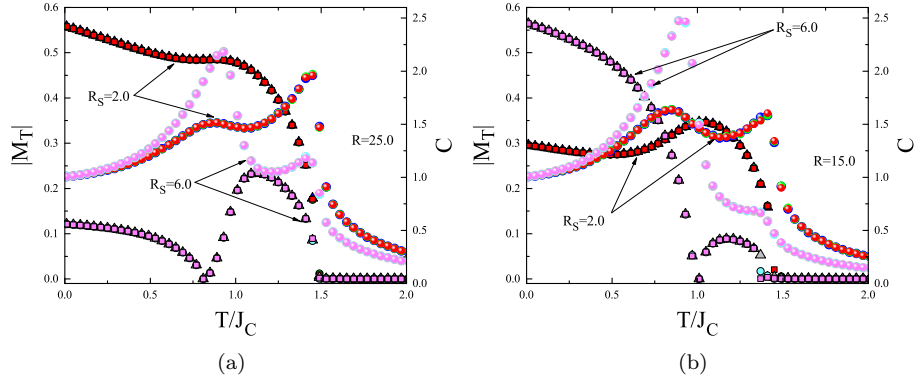


FIG. 9: Temperature dependence of the total magnetization $|M_T|$ and specific heat C for the particles enlisted in Table I. The system parameters are selected as $J_S = 0.5J_C$, $J_{IF} = -0.5J_C$, $K_C = 0.1J_C$, $K_S = 1.0J_C$. The curves corresponding to three different degrees of roughness with $\sigma = 0.01, 0.5$ and 1.0 overlap with each other.

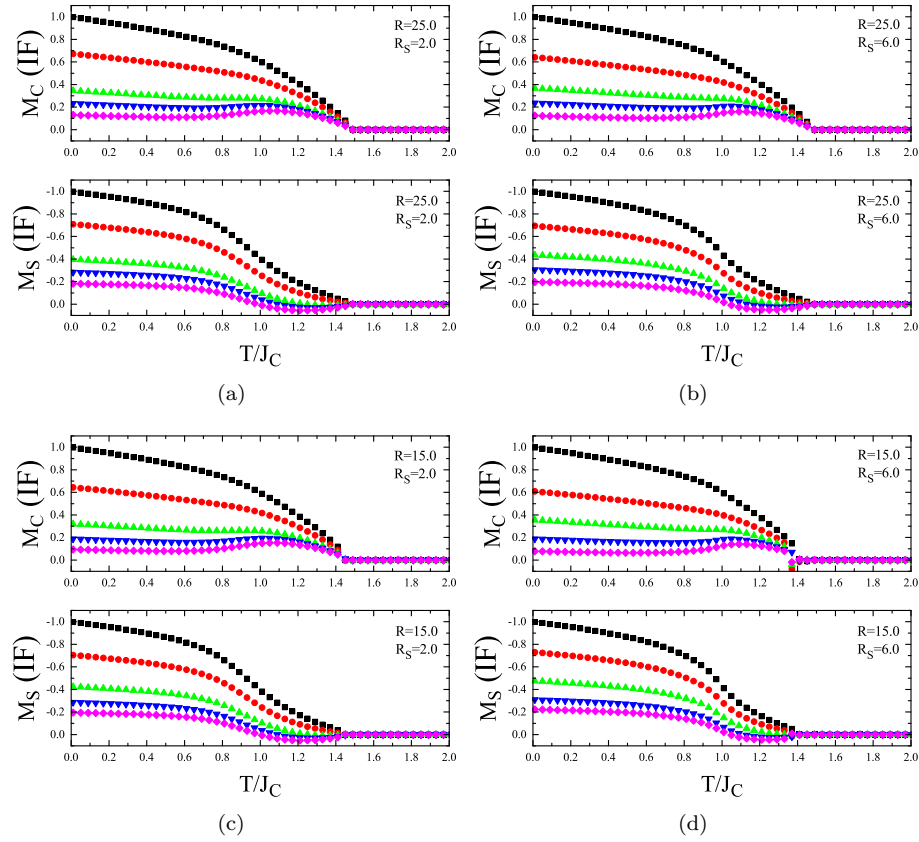


FIG. 10: Thermal variation of the interface magnetization coming from the core and shell parts for particles prepared as (a) sample 1, (b) sample 2, (c) sample 3, and (d) sample 4. Different symbols correspond to different degrees of roughness such as $\sigma = 0.01$ (■), $\sigma = 0.1$ (●), $\sigma = 0.2$ (▲), $\sigma = 0.3$ (▼), $\sigma = 0.5$ (◆). The system parameters are as follows: $J_S = 0.5J_C$, $J_{IF} = -0.5J_C$, $K_C = 0.1J_C$, $K_S = 1.0J_C$.

- For particles with diluted interface, our numerical results indicate that there exists a region in the disorder spectrum where compensation temperature linearly decreases with decreasing dilution parameter. It is interesting to note that the linear variation region becomes narrower for bigger particles.
- It is found that the degree of roughness at the interface of the particle does not play any significant role on the variation of both the compensation point and critical temperature. However, the low temperature saturation magnetizations of the core and shell interface regions sensitively depend on the roughness parameter.

As a final conclusion, we note that more work is required to match and understand the theoretical and experimental findings regarding the thermal and magnetic properties of the advanced functional core-shell nanoparticles in different geometries.

Acknowledgements

The numerical calculations reported in this paper were performed at TUBITAK ULAKBIM High Performance and Grid Computing Center (TR-Grid e-Infrastructure).

-
- [1] A.E. Berkowitz, R.H. Kodama, S.A. Makhlof, F.T. Parker, F.E. Spada, E.J. McNiff Jr., and S. Foner, *J. Magn. Magn. Mat.* **196**, 591 (1999).
- [2] T. Hayashi, S. Hirono, M. Tomita, and S. Umemura, *Nature* **381**, 772 (1996).
- [3] D. Guo, G. Xie, and J. Luo, *J. Phys. D: Appl. Phys.* **47**, 013001 (2014).
- [4] Q.A. Pankhurst, J. Connolly, S.K. Jones, and J. Dobson, *J. Phys. D: Appl. Phys.* **36**, R167 (2003).
- [5] K. McNamara, and S.A.M. Tofail, *Advances in Physics: X* **2:1**, 54 (2017).
- [6] Y.P. Ivanov, A. Alfadhel, M. Alnassar, J.E. Perez, M. Vazquez, A. Chuvilin, and J. Kosel, *Sci. Rep.* **6**, 24189 (2016).
- [7] P. Bhatt, A. Kumar, S.S. Meena, M.D. Mukadam, and S.M. Yusuf, *Chem. Phys. Lett.* **651**, 155 (2016).
- [8] B. Martínez, X. Obradors, LL. Balcells, A. Rouanet, and C. Monty, *Phys. Rev. Lett.* **80**, 181 (1998).
- [9] M. Estrader, A. López-Ortega, S. Estradé, I.V. Golovsky, G. Salazar-Alvarez, M. Vasilakaki, K.N. Trohidou, M. Varela, D.C. Stanley, M. Sinko, M.J. Pechan, D.J. Keavney, F. Peiró, S. Suriñach, M.D. Baró, and J. Nogués, *Nat. Commun.* **4**, 2960 (2013).
- [10] R.N. Bhowmik, *J. Magn. Magn. Mater.* **323**, 311 (2011).
- [11] P.K. Manna, and S.M. Yusuf, *Phys. Rep.* **535**, 61 (2014).
- [12] M. Kiwi, *J. Magn. Magn. Mater.* **234**, 584 (2001).
- [13] J. Nogués, J. Sort, V. Langlais, V. Skumryev, S. Suriñach, J. S. Muñoz, and M. D. Baró, *Phys. Rep.* **422**, 65 (2005).
- [14] A. Berkowitz, and K. Takano, *J. Magn. Magn. Mater.* **200**, 552 (1999).
- [15] Ó. Iglesias, A. Labarta, and X. Battle, *J. Nanosci. Nanotechnol.* **8**, 2761 (2008).
- [16] L. Néel, *Ann. Phys. Paris* **3**, 137 (1948).
- [17] P. Hansen, *J. Appl. Phys.* **62**, 216 (1987).
- [18] G.M. Buendia, and E. Machado, *Phys. Rev. B* **61**, 14686 (2000).
- [19] H.-P.D. Shieh, and M.H. Kryder, *Appl. Phys. Lett.* **49**, 473 (1986).
- [20] M. Mansuripur, *J. Appl. Phys.* **61**, 1580 (1987).
- [21] T. Kaneyoshi, *Phys. Status Solidi B* **248**, 250 (2011).
- [22] T. Kaneyoshi, *Physica A* **390**, 3697 (2011).
- [23] N. Zaim, A. Zaim, and M. Kerouad, *Solid State Commun.* **246**, 23 (2016).
- [24] N.R. Anderson, and R.E. Camley, *Phys. Rev. B* **94**, 134432 (2016).
- [25] R.F.L. Evans, D. Bate, R.W. Chantrell, R. Yanes, and O. Chubykalo-Fesenko, *Phys. Rev. B* **84**, 09204 (2011).
- [26] R.F.L. Evans, R.W. Chantrell, and O. Chubykalo-Fesenko, *MRS Bulletin* **38**, 909 (2013).
- [27] L.B. Ho, T.N. Lan, and T.H. Hai, *Physica B* **430**, 10 (2013).
- [28] Z. Mao, X. Zhan, and X. Chen, *J. Phys.: Condens. Matter* **24**, 276002 (2012).
- [29] V. Dimitriadis, D. Kechrakos, O. Chubykalo-Fesenko, and V. Tsiantos, *Phys. Rev. B* **92**, 064420 (2015).
- [30] T. Kaneyoshi, *J. Phys.: Condens. Matter.* **3**, 4497 (1991).
- [31] D. Hinzke, and U. Nowak, *Comput. Phys. Commun.* **121-122**, 334 (1999).
- [32] G. Marsaglia, *Ann. Math. Stat.* **43**, 645 (1972).
- [33] R.F.L. Evans, W.J. Fan, P. Chureemart, T.A. Ostler, M.O.A. Ellis, and R.W. Chantrell, *J. Phys.: Condens. Matter* **26**, 103202 (2014).
- [34] M.E.J. Newman, and G.T. Barkema, *Monte Carlo Methods in Statistical Physics*, Clarendon Press, Oxford, 2001.
- [35] T. Miyazaki, H. Jin 2012 *The Physics of Ferromagnetism* (Springer Series in Materials Science 158); S. Chikazumi, 1997 *The Physics of Ferromagnetism* (Oxford Science Publications 94);
- [36] Here, instead of critical temperatures observed in the thermodynamic limit, we mean a pseudo critical one, since we are dealing with a finite particle.
- [37] If a magnetic system exhibits compensation phenomenon then the spontaneous total magnetization reverses its sign at a particular temperature called as the compensation temperature.